


FULL PAPER

Open Access



MASCOT's in situ analysis of asteroid Ryugu in the context of regolith samples and remote sensing data returned by Hayabusa2

Katharina Otto^{1,2*} , Tra-Mi Ho³, Stephan Ulamec⁴, Jean-Pierre Bibring⁵, Jens Biele⁴, Matthias Grott¹, Maximilian Hamm^{1,6}, David Hercik⁷, Ralf Jaumann⁶, Masahiko Sato⁸, Stefan E. Schröder⁹, Satoshi Tanaka¹⁰, Ulrich Auster¹¹, Kohei Kitazato¹², Jörg Knollenberg¹, Aurelie Moussi¹³, Tomoki Nakamura¹⁴, Tatsuaki Okada¹⁰, Cedric Pilorget⁵, Nicole Schmitz¹, Seiji Sugita⁸, Koji Wada¹⁵ and Hikaru Yabuta²

Abstract

The Hayabusa2 mission provided a unique data set of asteroid Ryugu that covers a wide range of spatial scale from the orbiter remote sensing instruments to the returned samples. The MASCOT lander that was delivered onto the surface of Ryugu aimed to provide context for these data sets by producing in situ data collected by a camera (MasCam), a radiometer (MARA), a magnetometer (MasMag) and a spectrometer (MicrOmega). In this work, we evaluate the success of MASCOT as an integrated lander to bridge the gap between orbiter and returned sample analysis. We find that MASCOT's measurements and derivatives thereof, including the rock morphology, colour in the visible wavelengths, possible meteorite analogue, density, and porosity of the rock at the landing site are in good agreement with those of the orbiter and the returned samples. However, it also provides information on the spatial scale (sub-millimetres to centimetres) at which some physical properties such as the thermal inertia and reflectance undergo scale-dependent changes. Some of the in situ observations such as the presence of clast/inclusions in rocks and the absence of fine particles at the landing site was uniquely identified by MASCOT. Thus, we conclude that the delivery of an in situ instrument like MASCOT provides a valuable data set that complements and provides context for remote sensing and returned sample analyses.

Keywords Asteroid Ryugu, In situ analyses, Asteroid sample return, Multi-scale analysis, Asteroid regolith properties, Asteroid regolith, MASCOT, Hayabusa2

*Correspondence:

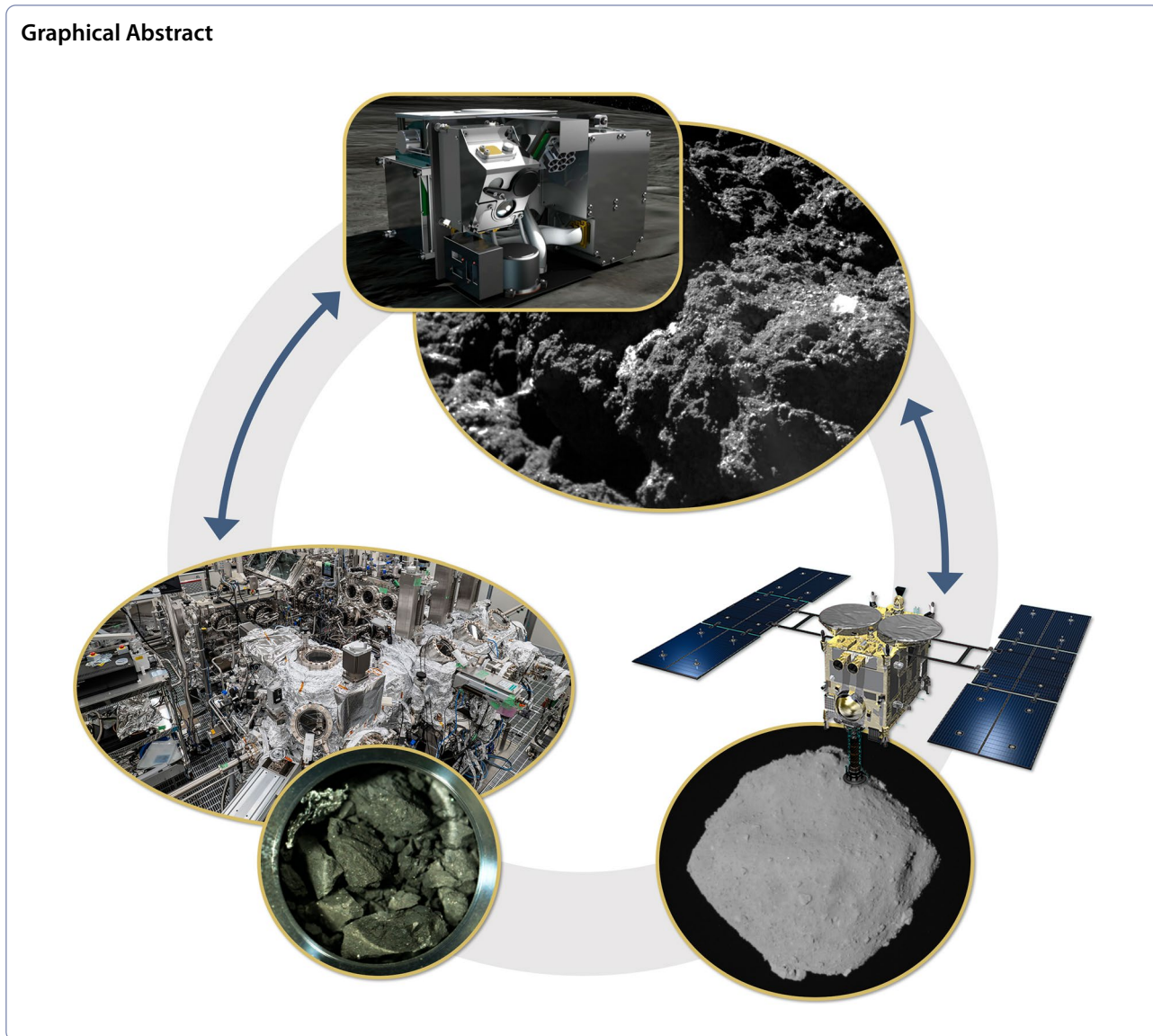
Katharina Otto

katharina.otto@dlr.de

Full list of author information is available at the end of the article



© The Author(s) 2023. **Open Access** This article is licensed under a Creative Commons Attribution 4.0 International License, which permits use, sharing, adaptation, distribution and reproduction in any medium or format, as long as you give appropriate credit to the original author(s) and the source, provide a link to the Creative Commons licence, and indicate if changes were made. The images or other third party material in this article are included in the article's Creative Commons licence, unless indicated otherwise in a credit line to the material. If material is not included in the article's Creative Commons licence and your intended use is not permitted by statutory regulation or exceeds the permitted use, you will need to obtain permission directly from the copyright holder. To view a copy of this licence, visit <http://creativecommons.org/licenses/by/4.0/>.



Introduction

Hayabusa2 is a mission by the Japan Aerospace Exploration Agency (JAXA) that was launched in December 2014 to the near-Earth asteroid (162,173) Ryugu. After arrival at the asteroid in June 2018 and an observation phase that not only included remote observations but also the delivery of the MINERVA II and MASCOT landers (Lange et al. 2020), as well as an impact experiment (Arakawa et al. 2020), samples were returned to Earth in December 2020. These samples can now be put into context with the observations at and on the asteroid.

The small, agile Mobile Asteroid Surface Scout, MASCOT (Fig. 1), was delivered by the Hayabusa2 main spacecraft to the surface of Ryugu on October 3rd, 2018 to perform in-situ measurements on the surface of the

asteroid (Jaumann et al. 2019; Ho et al. 2021). There, it landed in front of a rough-looking rock of approximately 15 cm in size free of fine-grained deposits (Fig. 2). Instead, bright spots, potentially inclusions, were visible on the rock surface (Fig. 3) (Jaumann et al. 2019).

While the main objectives of the Hayabusa2 mission were to understand the origin and evolution of materials in the early solar nebula and in a C-type asteroid, Ryugu (Watanabe et al. 2017), MASCOT was to focus on in situ science, including the measurement of physical properties of the surface material and high-resolution imaging of undisturbed surface material (Ho et al. 2017). The combination of remote sensing from the main spacecraft, in situ surface measurements by landers, and returned sample analysis allow the Hayabusa2 mission to conduct

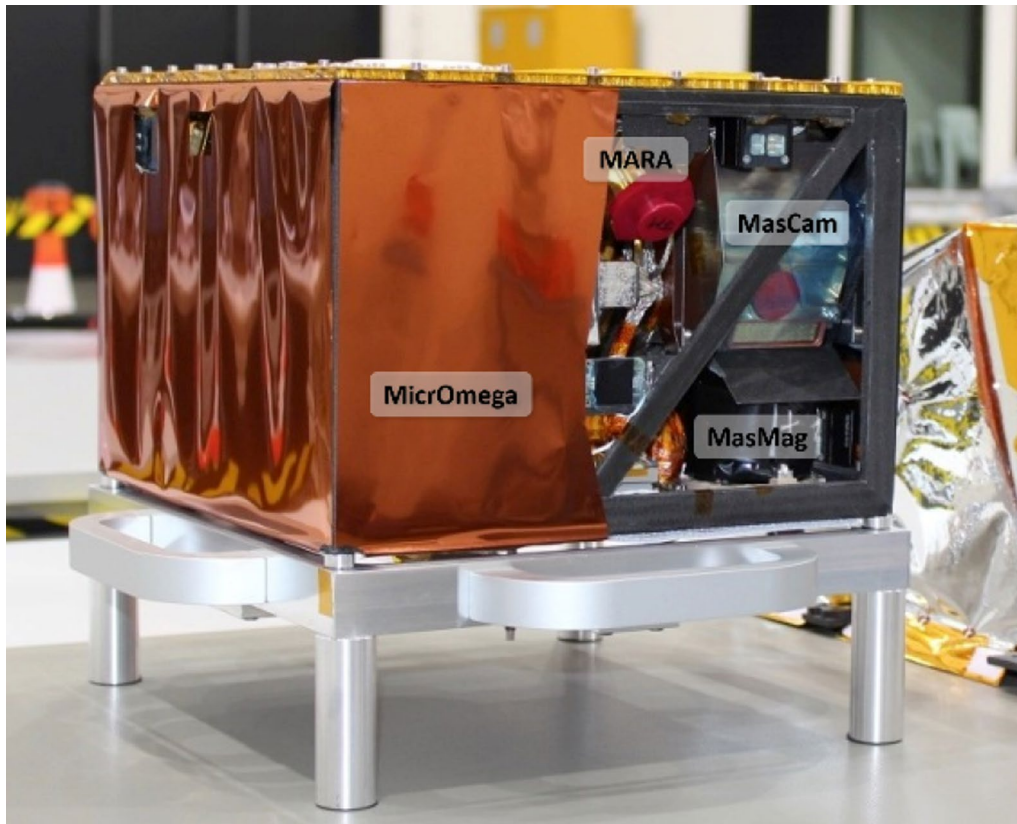


Fig. 1 Photo of the MASCOT lander with its scientific instruments labeled. Note that MIRA and MasCam have overlapping field of views

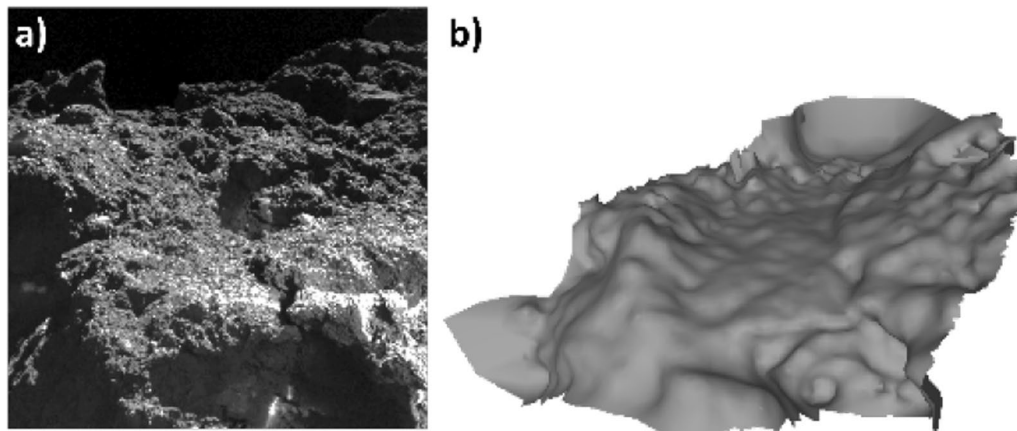


Fig. 2 **a** MASCOT’s landing site imaged by MasCam at day time and **b** shape model of the scene. The scene is approximately 25 cm across. The illuminated flat plateau (~ 15 cm across) is referred to as the MASCOT rock. The overexposed streaks in the foreground in **a**) are reflections of MASCOT’s housing

global-, local-, and micro-scale observations. Thus, MASCOT bridges the gap between the samples returned and the orbiter observations (Ho et al. 2017, 2021).

MASCOT has a payload of four scientific instruments: a camera, MasCam, which resolved structures near the

landing site with a spatial pixel resolution of up to 200 μm (Jaumann et al. 2017), a radiometer, MIRA, to measure thermal emission of the surface during a day–night cycle and thus determine the thermal conductivity of surface material (Grott et al. 2017), a hyperspectral near-infrared

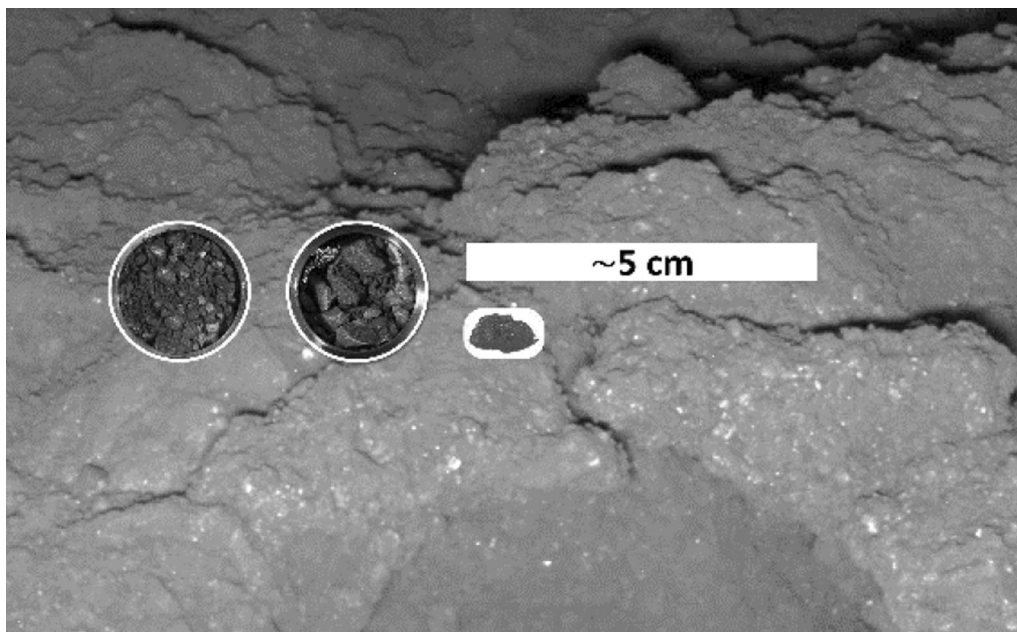


Fig. 3 Rock illuminated by MasCam's red LED at night in relation to the returned sample. Sub-millimetre-sized bright spots are clearly visible in the front. The two circles illustrate the ~ 1.7 cm across opening of the sample holders with the returned samples. The largest returned fragment (C9000) with 1 cm in size is also shown for reference. Due to the distortion in the MasCam image, the dimensions of the samples and the MASCOT scene are only approximately to scale at this indicated location. Please note that the samples were not collected at this site and are shown here for reference only. The images of the samples were retrieved from (Astromaterials Science Research Group (ASRG) 2022)

(NIR) microscope, MicrOmega, designed to determine the surface mineralogical and molecular composition at the grain scale (Bibring et al. 2017), and a magnetometer, MasMag, to search for any sign of possible remnant magnetization (Herčík et al. 2017) (Fig. 1). With the exception of the magnetometer MasMag, MASCOT's instruments have corresponding orbiter instruments: A telescopic camera (ONC (Kameda et al. 2017)), a thermal mapper (TIR (Okada et al. 2017)) and a spectrometer (NIRS3 (Iwata et al. 2017)). An overview of the MASCOT lander design is given by Ho et al. (2017), while the actual mission activities including the on-asteroid operations is summarised by (Ho et al. 2021).

Unfortunately, MASCOT landed on a depression with the consequence that the surface to be characterized was too far away to be illuminated and imaged by MirOmega (Bibring et al. 2022). Nevertheless, an instrument identical to MicrOmega has been applied in the curatorial work of the returned Ryugu samples and revealed sub-millimetre chemical heterogeneities including carbonates and NH-rich compounds (Pilorget et al. 2022).

On December 6th, Hayabusa2 returned samples from Ryugu to Earth. The samples were collected from two sites on Ryugu and stored in separate sample containers. Chamber A contained (3.237 ± 0.002) g surface material from Ryugu's equatorial ridge and Chamber C contained (2.025 ± 0.003) g of surface and potentially subsurface

material collected near an artificial crater created by Hayabusa2's SCI impact experiment (Arakawa et al. 2020; Yada et al. 2022). The samples are composed of predominantly millimetre-sized particles embedded in fine sub-millimetre dust, with the largest fragment being ~ 8 mm across (Yada et al. 2022). Preliminary investigations indicate that the collected samples are representative of Ryugu's surface based on their colour, shape and structure (Pilorget et al. 2022; Tachibana et al. 2022).

In this paper, we discuss the extent to which conclusions from the measurements performed in situ at the surface of Ryugu have been confirmed by ongoing sample analysis, as well as how in situ data on undisturbed material on the asteroid surface can enhance the interpretation of the returned samples.

In situ observations

Observations with MasCam

MASCOT's MasCam is a scientific camera equipped with a Scheimpflug optic that allows it to image the entire scene along the camera's depth of field (150 mm to infinity) in focus. In addition, MasCam had the ability to illuminate Ryugu's surface with an array of light-emitting diodes (LEDs), equipped with 4×36 monochromatic LEDs working in four spectral bands (Jaumann et al. 2017). MasCam took images both during descent and on the surface with scales down to 0.1 mm/pixel (Jaumann

et al. 2019). These observations revealed a number of important properties of Ryugu, most of which were unexpected before landing. As already identified in Hayabusa2 ONC images, two types of boulders are clearly distinguished in lower resolution MasCam descent images: brighter ones with smooth surfaces, non-dendritic fractures and modified by a process that has resulted in both sharp edges and rounded structures, and darker ones with cauliflower-like surfaces and characteristics suggestive of thermal-fatigue. Boulder sizes range from a few millimetres to a few tens of metres and the sorting of grains, pebbles and boulders is poor. The relatively large sizes of boulders and their different morphologies reflected by the two boulder types described above suggest that they may be fragments from Ryugu's parent body/bodies that reaccumulated to form Ryugu itself and reflect heterogeneities in Ryugu's parent body/bodies (Jaumann et al. 2019).

At the location of $22.32^{\circ}\text{S} \pm 0.05^{\circ}/317.16^{\circ}\text{E} \pm 0.05^{\circ}$, MASCOT came to rest on Ryugu's surface and the fine structure of boulders imaged there at the highest resolution exhibit a matrix with sub-millimetre size inclusions and morphologies similar to carbonaceous chondrites.

In the context of the Ryugu rock, the word "inclusion" has been used to describe bright spots surrounded by a darker matrix (Fig. 3) (Schröder et al. 2021; Otto et al. 2021). Given the limitation in actually identifying the composition and structure of these spots, the term "clast" as used in sedimentary geology may also be adequate. To maintain consistency with previous publications, we will call the bright spots surrounded by a darker matrix "inclusions" in this article.

No accumulation of fine dust is identified in the MasCam images. Close-up observations show the presence of inclusions (Jaumann et al. 2019; Schröder et al. 2021; Otto et al. 2021). Small inclusions have the characteristic size (sub-millimetre) of chondrules, whereas the larger ones may be refractory, calcium–aluminium-rich inclusions (CAI). This suggests that Ryugu's material has experienced heating but is not fully hydrated, which is consistent with the absence of the $0.7\ \mu\text{m}$ absorption feature in ground-based reflectance spectra, confirmed by ONC (Tatsumi et al. 2021). The visible colours of the inclusions provide compositional clues, but their interpretation is limited by the lack of reflectance data in the IR wavelength range, where most bands that are diagnostic for the mineralogy are located. However, the spectral characteristics of the inclusions are similar to those in carbonaceous chondrites (Schröder et al. 2021; Otto et al. 2021). A systematic comparison of the inclusions' size distribution, relative spectral slope and brightness relative to the matrix, and the matrix volume abundance imaged within the rock on Ryugu and a set

of carbonaceous chondrites including CM2, CO3, CV3 and CK3 revealed that Ryugu's rock fits well within the parameter space of these meteorites. However, Ryugu's material tends to have slightly larger inclusions and a higher matrix volume abundance (Schröder et al. 2021; Otto et al. 2021). MasCam also allowed the derivation of the surface roughness on small spatial scales (sub-millimetre) by applying a shadow tracing method to the images taken at night when the scene as illuminated with MasCam's LEDs. The result showed that Ryugu's rock surface has a fractal dimension of 1.16 ± 0.04 and a root mean square (RMS) slope of $36.6^{\circ} \pm 1.4^{\circ}$. It thus appears less rough ($\sim 6\%$) compared to material imaged on comet 67P/Churyumov-Gerasimenko (Otto et al. 2020). The difference in roughness may be explained by the different processes altering the surfaces of asteroids and comets. While sublimation of volatiles seems to be the main process to generate roughness on comets, micrometeoroid bombardment, thermal fracturing and solar weathering may play a significant role in shaping asteroid surfaces (Otto et al. 2020).

Observations with MARA

The MASCOT radiometer MARA is an instrument that measured radiative flux emitted from the surface of Ryugu in the thermal infrared wavelength range in six dedicated channels (Grott et al. 2017). MARA operated during the entire MASCOT mission starting at MASCOT's separation from the Hayabusa2 spacecraft and gathered data throughout the 17 h of operation (Ho et al. 2021). After landing, MARA measured emitted flux of a rock at the MASCOT landing site over the period of a full asteroid rotation (7:38 h). Two of MARA's infrared channels were dedicated to measuring low night time temperatures, and a bandpass filter between 8 and $12\ \mu\text{m}$ as well as a $>3\ \mu\text{m}$ long pass filter were employed for this purpose. Four additional bandpass channels in the 5.5–7, 8–9.5, 9.5–11.5, and 13.5–15.5 μm wavelength range were dedicated to recording emissivity as a function of wavelength and to constrain surface composition. MARA's field of view covers about 10–15 cm^2 and is within MasCam's view (Grott et al. 2017; Hamm et al. 2018).

At the landing site, asteroid surface temperatures were found to vary between 210 and 300 K based on measurements in the 8–12 μm wavelength range (Grott et al. 2019). Using a thermophysical model of the asteroid and taking surface roughness into account, the thermal inertia of the rock was found to be $282^{+93}_{-25}\ \text{J m}^{-2}\ \text{K}^{-1}\ \text{s}^{-1/2}$ (Hamm et al. 2018; Grott et al. 2019), a value similar to the $(225 \pm 45)\ \text{J m}^{-2}\ \text{K}^{-1}\ \text{s}^{-1/2}$ later found to be globally representative for Ryugu's boulders and surrounding material based on Hayabusa2 TIR data (Okada et al.

2020; Shimaki et al. 2020). As there was no indication for a masking layer of surface dust (Biele et al. 2019), the low thermal inertia derived from MARA data was interpreted to be caused by a high intrinsic (micro-)porosity of the rock. Thus, porosities between 0.28 and 0.55 were derived based on an extrapolation of laboratory data for the thermal conductivity of meteorites as a function of porosity (Grott et al. 2019). A re-analysis of the MARA data set using data assimilation techniques narrowed down the range of uncertainties to thermal inertias around $(295 \pm 18) \text{ J m}^{-2} \text{ K}^{-1} \text{ s}^{-1/2}$ and porosities between 0.30 and 0.52 (Hamm et al. 2020). With the availability of a detailed shape model of the MASCOT rock (Scholten et al. 2019) (Fig. 2b) to refine thermal re-radiation and illumination conditions, and taking into account the effect of sunlight reflection casted by MASCOT into the MARA field of view (Fig. 2a), the data were re-analysed (Hamm et al. 2022). The thermal inertia was found to be lower with $256 \pm 34) \text{ J m}^{-2} \text{ K}^{-1} \text{ s}^{-1/2}$ and porosity between 0.46 and 0.56 depending on the empirical model used to relate porosity and thermal conductivity (Krause et al. 2011; Flynn et al. 2018). Based on estimates of Ryugu's packing state and the constraint posed by Ryugu's bulk density, porosities around 0.50 ± 0.02 were later favoured using semi-empirical mixing models (Grott et al. 2020). Such porosities imply grain densities of $(2848 \pm 152) \text{ kg m}^{-3}$, values similar to those found in CM meteorites as well as CI Tagish Lake (Grott et al. 2020).

The infrared emissivity in the MARA bandpass channels was estimated by combing the thermal model of a rock with a data assimilation scheme (Hamm et al. 2022). The emissivity estimates were compared to spectra of thin sections of powder samples of meteorites. These data show that the spectral variation of the rock's emissivity shares similarities with the bulk samples of the most aqueously altered meteorites (CI, CM, and CR carbonaceous chondrites), indicating Ryugu experienced strong aqueous alteration prior to any dehydration.

Observations with MasMag

The MASCOT magnetometer MasMag is a triaxial flux-gate magnetometer which acquired data from the beginning of the lander descent, through the several bounces, touchdown and at the final resting position (Hercik et al. 2020). The descent profile of the observed magnetic field, after calibration and de-spinning, does not show any detectable change in the magnetic field above the background level. The observed magnetic field vector fluctuates within a $\pm 1 \text{ nT}$ range and no systematic change was visible when approaching the surface down to $\sim 10 \text{ cm}$ (distance of the sensor to the surface at resting position). Such behaviour directly excludes any global magnetic field and larger magnetization down to metre-scales.

However, based on the accuracy of the measurement, we can assess the upper limit of the magnetization under certain assumptions. The specific magnetic moment (level of magnetization) is the effective magnetic moment (Am^2) per kg of the material. Measuring this parameter assumes, a priori, a homogeneous magnetization through the sample. If the material was built from smaller magnetized particles, e.g., in a process of accretion and coagulation, the mutual orientation of the domains would be random and the contributions from magnetized individual domains would cancel each other. The total magnetic moment of the bulk is then negligible, while the domains themselves can retain high levels of magnetization. Therefore, we speak about the magnetization scale as the representative scale at which the material is homogeneously (unidirectionally) magnetized. Microscopic observation of the returned samples revealed that the Ryugu particles were composed of lithologically different domains of several 100 s of micrometre in size (Nakamura et al. 2022). Assuming a magnetization scale of centimetre sized domains within a material with a density of 1200 kg/m^3 leads to an upper limit of the specific magnetic moment on the order of $10^{-2} \text{ Am}^2/\text{kg}$. The investigations of chondrite meteorites show the natural remnant magnetization from 10^{-4} to $10^{-2} \text{ Am}^2/\text{kg}$ (Terho et al. 1996; Gattacceca and Rochette 2004). This agrees with MasMag's measurement and is to be further refined by magnetization analysis of the returned samples (see section below).

However, it shall be noted that there is a discrepancy between the meteorite measurements, which in general show bulk magnetization (even on $>10 \text{ cm}$ scales) and the measurements on solar system bodies. So far, only three magnetic measurements were performed on the surface of small bodies: Ryugu, S-type asteroid Eros (Acuña et al. 2002) and comet 67P/Churyumov-Gerasimenko (Auster et al. 2015). All three measurements show no magnetic signal that can be directly related to the body or the regolith. At least in case of Ryugu and comet 67P/Churyumov-Gerasimenko, the discrepancy could be that the pristine material has rather low coherence (tensile strength), which might prevent the material to reach the Earth's surface. The fact that Ryugu's samples contain no chondrules and that the material has a very low grain density of 1380 kg/m^{-3} and tensile strengths, leads to the conclusion that Ryugu is not lithified enough to survive atmospheric entry (Herbst and Greenwood 2022). Consequently, we may not have a representative meteorite sample on Earth, although initial sample analysis revealed that Ryugu's mineralogy is similar to CI chondrites (Tsuchiyama et al. 2022). Therefore, it is not excluded that future observations will reveal small bodies

with significant magnetic signatures, as it is expected for metal-rich asteroid types.

MASCOT results in context of orbiter instruments

The Hayabusa2 orbiter was also equipped with a telescopic camera (ONC), a Spectrometer (NIRS3) and a radiometer (TIR) that allow a cross interpretation of MASCOT data and orbiter data spanning multiple spatial scales (Ho et al. 2021).

Within the landing site of MASCOT, MasCam confirmed two of the four types of rock morphologies identified in the ONC images of Hayabusa2 (Sugita et al. 2019): the dark and rough type 1 boulders and the bright and smooth type 2 boulders (Jaumann et al. 2019). In addition, MasCam provided close-up fine-scale texture identification. Sugita et al. (2019) derived from their data that the rugged surfaces and edges of the type 1 boulders showed uneven layered structures that could be related to the inclusion of coarse-grained clasts. This assumption is supported by the high-resolution of the MasCam images, in which the mm-size structure of type 1 boulder results in a granular friable surface texture (Jaumann et al. 2019). The images of MasCam at the MASCOT landing site revealed a rock with a cauliflower-like surface texture consisting of undulations of ~ 1 cm scale and 2–3 mm scale. This topographic surface roughness at the sub-millimetre scale could be quantified by surface roughness parameters (Otto et al. 2020). Compared with roughness values derived from thermal modelling of Ryugu's surface, the small-scale analysis of Ryugu's rock revealed a lower RMS slope of $36.6^\circ \pm 1.4^\circ$ compared to $47^\circ \pm 5^\circ$ (Shimaki et al. 2020; Otto et al. 2020). Applying the image analysis technique to a global image of Ryugu and deriving the RMS slope from MARA day time measurements through fitting the thermal model to the measured data also reveal lower RMS values ($32.9^\circ \pm 2.2^\circ$ and 28.6° , respectively) (Otto et al. 2020). The discrepancy between these values can be explained by the different methods to derive the RMS slope and reflects the dependence of the roughness parameters on the spatial scale on which they are derived.

MARA results serve as an important anchoring point for the interpretation of global thermal imaging data, which was provided by Hayabusa2's TIR instrument. TIR data indicate boulders, such as observed by MasCam during MASCOT's descent, cover a large part of Ryugu's surface and only a minority of boulders were found to have thermal inertias exceeding $600 \text{ J m}^{-2} \text{ K}^{-1} \text{ s}^{-1/2}$, which is similar to that of typical dense carbonaceous chondrites (Okada et al. 2020). A thermal inertia of $(225 \pm 45) \text{ J m}^{-2} \text{ K}^{-1} \text{ s}^{-1/2}$ was found to be globally representative for Ryugu (Okada et al. 2020; Shimaki et al. 2020). Therefore, the majority of boulders as well as the

surrounding large (> 10 cm) rock fragments are interpreted to be highly porous (Okada et al. 2020), consistent with estimates of inter-boulder porosity of about 16% (Grott et al. 2020) and a bulk porosity of approximately 50–60% (Watanabe et al. 2019).

MASCOT was able to complement the Hayabusa2 orbiter data with necessary constraints by providing local high-resolution data. For example, the presence of a dust-free surface, small scale surface texture, the thermal inertia of an individual rock sample or the lack of magnetization were delivered by MASCOT (Ho et al. 2021). In particular, the lack of a dust layer observed by MASCOT, significantly helped to interpret TIR orbiter data. Dust covering a rock influences the surface temperature and alters the apparent thermal inertia of the underlying material (Biele et al. 2019). This, could have led to the misinterpretation of TIR data. In addition, Shimaki et al. (2020) found that the area around MASCOT's landing site ($\sim 9 \times 9 \text{ m}^2$) has a 30% lower thermal inertia compared to MARA's measurements ($(200 \pm 7) \text{ J m}^{-2} \text{ K}^{-1} \text{ s}^{-1/2}$ and $(282 \pm 9535) \text{ J m}^{-2} \text{ K}^{-1} \text{ s}^{-1/2}$, respectively) indicating a scale dependence of the thermal inertia that could not have been detected without MASCOT. The application of this multi-scale analysis technique is promising for future planetary explorations.

A detailed comparison between orbiter and lander measurements and results can also be found in Ho et al. (2021). Table 1 summarizes the results of the sample analysis, MASCOT and the relevant orbiter instruments.

Sample analysis results in context of MASCOT observations

On December 6th, 2020, Hayabusa2 returned samples of the surface of Ryugu in two sample containers totalling 5.4 g of Ryugu material (Yada et al. 2022). The intense suite of analysis that these samples will have been undergoing also includes the determination of morphologic and physical properties (Tachibana 2019; Tanaka et al. 2022) which were previously derived from MASCOT data. This gives MASCOT the unique opportunity to link orbiter data and returned samples and relate these properties on different spatial scales. Table 1 summarizes the findings of MASCOT that have overlap with the Hayabusa2 orbiter instruments and the analysis of the returned samples. Figure 3 illustrates the spatial relation between the returned samples and the scene around MASCOT imaged by

Comparison with MasCam

The majority of particles returned from Ryugu are in the sub-millimetre size range, but there are also particles up to ~ 8 mm in size. Initial visual classification of fragments larger than 1 mm included two types of particles: 1) Rugged, predominantly round, and 2) smooth,

Table 1 Summary of the findings of the Hayabusa2 orbiter, MASCO_T, and the returned samples

Feature	Orbiter Observation	MASCO _T Observation	Returned Sample Observation
Particle size frequency distribution	Power index -2.65 for boulder > 5 m (Michikami et al. 2019) ^b	No particles observed ^d	Power index -3.88 for particles > 1 mm (Yada et al. 2022) ^b
Inclusions	Inclusions below detection limit	Bright inclusions of (0.63 ± 0.91) mm in size (Schröder et al. 2021) ^b	No inclusions (Chondrules/CA) observed but sub-millimetre sized grains of specific colour found (Ploigret et al. 2022) ^b
Surface structure/pebbles/boulders	Four types of boulders (dark and rugged, bright and smooth, bright and mottled, and Otohime Saxum) (Sugita et al. 2019), elongated impact fragments (Michikami et al. 2019) for metre sized boulders ^a	Two types of boulders (smooth, rough), locally rough surface texture (fractal dimension 1.18 (Otto et al. 2020)) ^a	Rugged and smooth as well as angular and round particles (Yada et al. 2022) elongated and sub-equant blocks with concave portions (Tsuchiyama et al. 2022; Tachibana et al. 2022b) in predominantly millimetre scale, flat saponite-rich surface layers (Nakamura et al. 2022) ^a
Colour in visible wavelength range	Consistent with C-complex asteroids (Sugita et al. 2019; Tatsumi et al. 2020) ^a	Neutral spectrum with individual inclusions with red or blue spectral slopes (Schröder et al. 2021) ^a	Overall slightly reddish slope, but with individual particles also being blue, consistent with C/Cb-type asteroids (Yumoto et al. 2022) ^a
Reflectance/albedo	Geometric albedo of 0.045 ± 0.002 (Sugita et al. 2019)/0.040 ± 0.005 at 0.55 μm (Tatsumi et al. 2020), Bond albedo of 0.014 ± 0.01 (Tatsumi et al. 2020) ^a	I/F of 0.034 ± 0.003 at 0.53 μm and phase angle 4.5° ± 0.1°, consistent with geometric albedo of 0.045 (Schröder et al. 2021) ^a	I/F at 0.55 μm and 30° phase angle is 30–70% higher than remote sensing observations, but darker than CI meteorites (Yumoto et al. 2022; Yada et al. 2022) ^b
Meteorite analogue	Thermally metamorphosed CI and/or shocked CM carbonaceous chondrites (Kitazato et al. 2019; Sugita et al. 2019) ^a	CI or CM carbonaceous chondrites based on inclusions characterization (Jaumann et al. 2019; Schröder et al. 2021; Otto et al. 2021), similar to CI based on thermal modelling (Hamm et al. 2022) ^a	CI chondrites but with lower albedo, higher porosity and more fragile characteristics as well as a lag of sulfates, ferrhydrites and interlayer water (Tanaka et al. 2022; Yada et al. 2022; Yokoyama et al. 2022; Ito et al. 2022) ^a
Thermal inertia	(225 ± 45) J m ⁻² K ⁻¹ s ^{-1/2} (Okada et al. 2020; Shimaki et al. 2020) ^a	(256 ± 34) J m ⁻² K ⁻¹ s ^{-1/2} at 230 K (Hamm et al. 2022) ^a	892 J m ⁻² K ⁻¹ s ^{-1/2} at a temperature of 298 K (Tanaka et al. 2022) ^b
Tensile strength	~229 kPa following the approach from Grott et al. (2019) (L ≈ 10 cm) ; Okada et al. (2020); Shimaki et al. (2020) ^a	200–280 kPa at a scale of ~ 10 cm assuming a Young's modulus representative of carbonaceous chondrites (Grott et al. 2019) ^a	4900 kPa (Tanaka et al. 2022) at a scale of 3 × 3 mm ^{2b}
Density ¹	Asteroid bulk density including microporosity of (1190 ± 20) kg/m ³ (Watanabe et al. 2019) ^a	Grain density of (2848 ± 152) kg/m ³ , bulk density of (1424 ± 135) kg/m ³ (Grott et al. 2020) and (1380 ± 70) kg/m ³ (Herbst et al. 2021) based on semi-empirical mixing models ^a	Sample bulk density of (1282 ± 231) kg/m ³ (Yada et al. 2022) and (1790 ± 80) kg/m ³ considering the full 3D structure (Nakamura et al. 2022) ^a
Porosity	Globally 0.3–0.5 (Okada et al. 2020), boulders with > 0.7 found on the floor of fresh craters (Sakatani et al. 2021) ^a	0.5 ± 0.02 (Grott et al. 2020) based on semi-empirical mixing models. 0.46 (Hamm et al. 2022) based on the model by Krause et al. (2011) ^a	Higher than CI chondrites, 0.46 based on typical CI grain densities (Yada et al. 2022; Nakamura et al. 2022) ^a
Homogeneous magnetization scale	n.a. ^c	Less than centimetre scale (Hercik et al. 2020) ^a	Roughly several 100s of micrometres (Sato et al. 2022; Nakamura et al. 2022) ^a
Specific magnetic moment	n.a. ^c	10 ⁻⁵ Am ² /kg for decimetre sized particles (Hercik et al. 2020) ^a	10 ⁻² Am ² /kg for 0.1–1 mm sized particles (Sato et al. 2022) ^a

¹ Bulk density = mass/volume, including cracks and pores; grain density = mass/volume, excluding cracks and pores (intrinsic material density)

^a Fields with bold text indicate an agreement of measurements

^b Fields with text in italics indicate a disagreement

^c If a comparison is not feasible, the text is not highlighted

angular particles (Yada et al. 2022) (Fig. 4a). During its descent, MasCam (as well as ONC) also identified such distinct types of boulders: a rough and dark and a smooth and comparatively brighter type. Thus, the morphologic heterogeneity appears to be present over a large spatial scale covering three orders of magnitude from millimetre scales of the returned samples to metre scales of the boulders on Ryugu. These different morphologic types and their distribution may hint at the presence of regolith with different degrees of material alteration (Jau-mann et al. 2019; Morota et al. 2020; Sakatani et al. 2021) and their mixing through impact gardening or regolith migration. The fact that the morphologic differences can

be traced down to the millimetre scale implies that the rough and smooth boulders' materials are physically different rather than being the product of, for example, varying exposure times to space weathering.

While the orbiter identified a boulder size frequency distribution with power index of -2.65 for boulders > 5 m (Michikami et al. 2019), the returned samples have a size frequency distribution with a power index of -3.88 for particles > 1 mm (Yada et al. 2022). The discrepancy may be caused by the different scales on which the measurements have been taken as well as the sampling, curation and/or delivering process (Yada et al. 2022). However, MasCam did not identify any pebbles (defined as the size

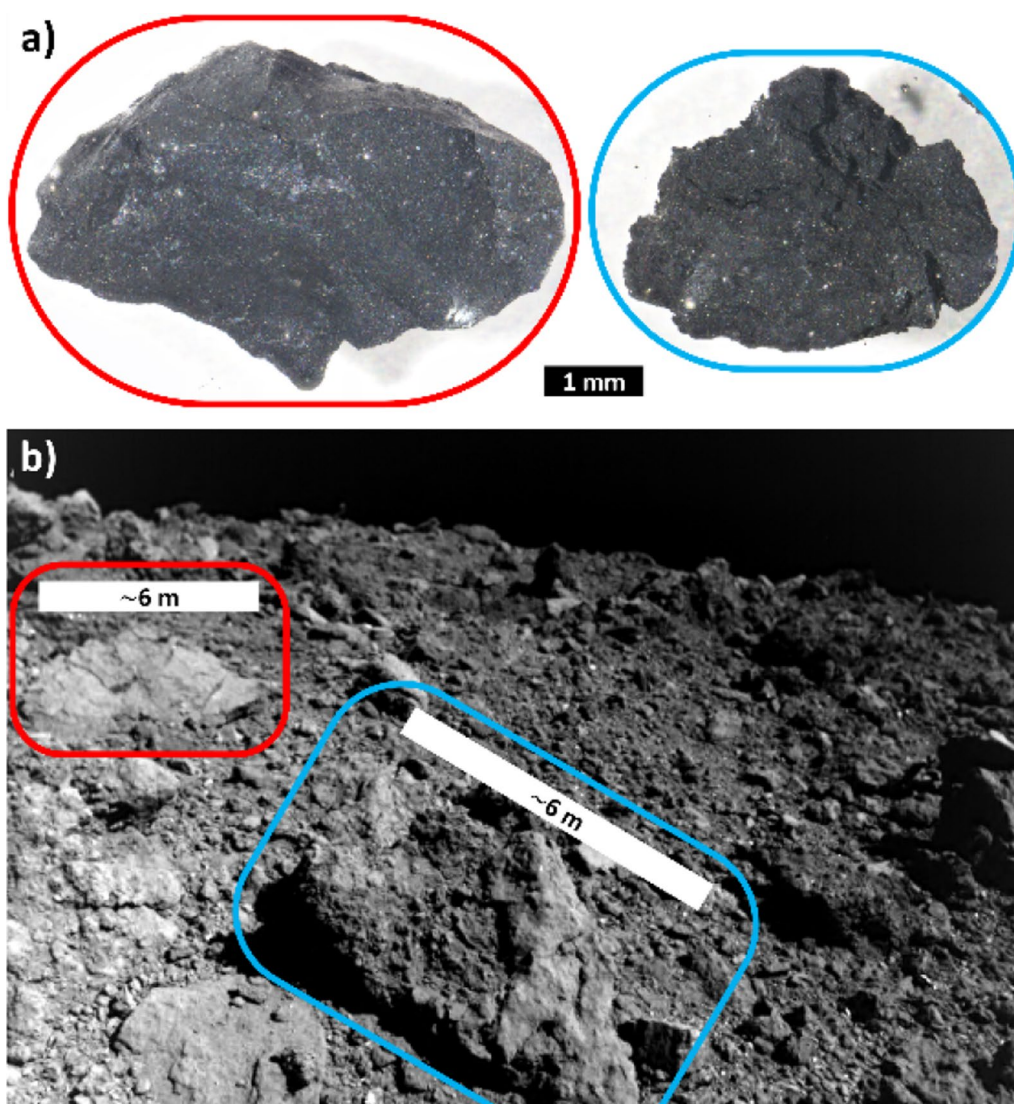


Fig. 4 **a** Two fragments of returned samples showing smooth (red) and rough (blue) surface textures and **b** smooth (red) and rough (blue) boulders imaged by MasCam during its descent. The scale bars are only approximately applicable at the indicated location. Note the different scale in a) and b). The shown fragments in a) are labeled C0005 (left) and C0008 (right) and were retrieved from the Hayabusa2, Ryugu Sample Curatorial Data Set (Astromaterials Science Research Group (ASRG) 2022)

range from 4 to 64 mm) or dust at its landing site. Instead MasCam imaged a dust-free, dark and rough rock (Fig. 2) nearby its landing site. Within this rock MasCam identified a number of bright millimetre-sized spots that were interpreted to be inclusions (e.g., CAI) as similar features are observed in some carbonaceous chondrites (Jaumann et al. 2019; Schröder et al. 2021; Otto et al. 2021). With a spatial resolution down to 0.1 mm/pixel, these features have sizes ranging between 0.2 mm and 5.4 mm in diameter (Schröder et al. 2021; Otto et al. 2021) and comprise about 7.6% of the rock imaged with the rest being darker matrix (Schröder et al. 2021). Their average size appears to be slightly larger than that of similar features common to carbonaceous chondrites (Otto et al. 2021). However, such inclusions could not be identified in the returned samples, in fact there are no intact CAI or chondrules in the returned samples even on the sub-millimetre scale (Yada et al. 2022; Nakamura et al. 2022), which reflects a high degree of aqueous alteration. However, Pilorget et al. (2022) report on the presence of bright isolated grains and structures on scales $< 50 \mu\text{m}$ that are comparable to MasCam's observations of bright spots. Most of these, however, fade to average brightness when changing the observation geometry, which was not possible to do with MasCam. Yumoto et al. (2022) explained the bright spots in the samples and the ones seen by MasCam as specular reflections and Nakamura et al. (2022) identified flat surfaces covered with a $2 \mu\text{m}$ thick saponite-rich layer that may cause such reflections. However, the large number as

well as the variation in colour of the bright spots seen by MasCam make this unlikely to be the sole explanation for the bright spots. It is more realistic that MasCam imaged inclusions (Schröder et al. 2022). The presence of inclusions in the rock imaged by MasCam and the lack of such features in the returned samples may hint that there are different types of material present on Ryugu, possibly originating from the two impacting parent bodies.

The Ryugu Sample Database (Astromaterials Science Research Group (ASRG) 2022) shows microscope images and photos of 704 individual returned particles between 0.6 mm and 10.3 mm in size. Although this collection may not be complete, some grains show distinct specular reflections and brighter patches in the sub-millimetre size range (e.g., A0038, A0136, A306, C0041). However, unlike inclusions, the brighter patches exhibit indistinct boundaries (Fig. 5). It is possible that MasCam imaged a rock with brighter patches similar to those seen in the returned samples, but did not resolve the boundary making a distinction between inclusions and areas with indistinct boundaries difficult.

Pilorget et al. (2022) show individual carbonate and NH-rich grains in the returned sample material. Although, the grains are not illustrated in the visible wavelengths at which MasCam operated, compositional heterogeneities appear to exist at the sub-millimetre scale. It is possible that such grains are fragments of larger grains that may have been shattered during the sampling process or the landing of the return capsule and

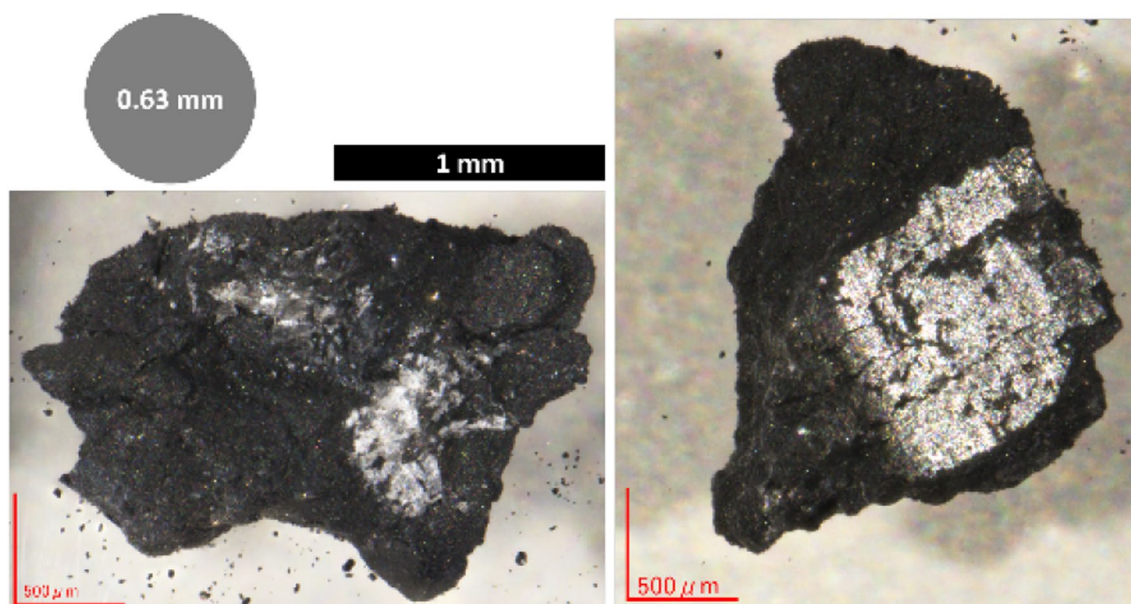


Fig. 5 Two examples of grains with brighter patches (left: C0041, right: A0038). The gray circle in the top left illustrates the average size of the inclusions identified by MasCam. The images are retrieved from the Hayabusa2, Ryugu Sample Curatorial Data Set (Astromaterials Science Research Group (ASRG) 2022)

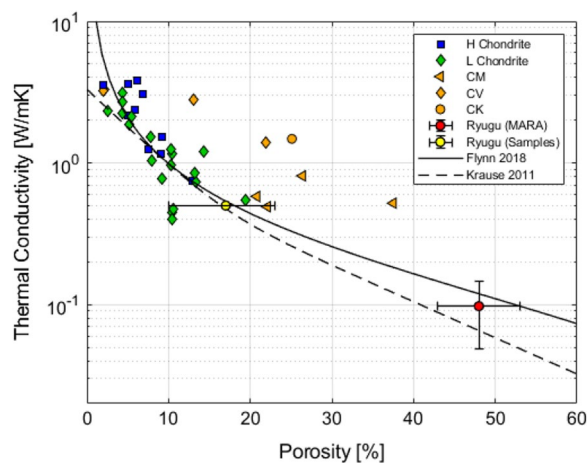


Fig. 6 Thermal conductivity as a function of porosity for different meteorite samples. For reference, the models proposed by Flynn et al. (2018) and Krause et al. (2011) are also shown. Thermal conductivity of the MASCOT rock was estimated based on the analysis of Hamm et al. (2022). Thermal inertia and thermal conductivity relate to each other following Eq. 1. The porosity and thermal conductivity for the Ryugu samples (Nakamura et al. 2022) is indicated

that these grains could have been identified as inclusions by MasCam.

Schröder et al. (2021) also investigated the colour and reflectivity of the inclusions imaged by MasCam in the visible wavelengths and found blue as well as red inclusions. These inclusions are up to two times brighter than the surrounding matrix, independent of their size or colour. A possible explanation for their colour may be the presence of phyllosilicates, Fe-rich oxides, or spinel which may give rise to a red slope and an enrichment in olivine may cause a blue appearance (Schröder et al. 2021). The spots imaged by MasCam have a mean diameter of 0.63 ± 0.91 mm, which is comparatively large in the context of other carbonaceous chondrites (Schröder et al. 2021; Otto et al. 2021). Yumoto et al. (2022) imaged the returned samples as a whole as well as 69 individual particles with sizes ranging between 1 and 7 mm at visible wavelengths corresponding to the ONC filters with a spatial resolution down to ~ 20 $\mu\text{m}/\text{pixel}$. They report on predominantly red sub-millimetre sized spots in the returned samples, which are up to ten times brighter than the average and ubiquitous on the returned samples. They argue that these spots, and similarly the red spots identified by MasCam, may be specular reflections, while the blue spots may be carbonate-rich inclusions. Other materials that could give rise to the spot-like bright appearance, such as sulphides, have also been detected within the returned samples (Nakamura et al. 2022).

Yumoto et al. (2022) and Schröder et al. (2021) also investigated the reflectivity in the visible wavelength of

the returned samples and the rock in front of MasCam, respectively. While Yumoto et al. (2022) found that the reflectance of some individual returned fragments is about 30–70% higher than that of global Ryugu as measured by ONC, Schröder et al. (2021) found a reflectance of the rock in front of MasCam in agreement with ONC observations. ONC measured the geometric albedo (phase angle of zero) at which no shadows are visible and MasCam imaged the rock at a low phase angle with almost no shadows, making the comparison straightforward (Schröder et al. 2021).

In general, the reflectance measured by ONC and the powdered returned samples agrees well. The fact that the average Ryugu observed by ONC is slightly brighter than the powdered samples (ratio of 0.9) may be attributed to the particle size of the samples (Nakamura et al. 2022). The dust covered surface on Ryugu before sample collection was brighter than the surface after the dust had been removed by the spacecraft thrusters during the sampling process (Morota et al. 2020). Given that the dust-free rock imaged by MasCam is not significantly darker than average Ryugu, this may imply that dust free surfaces similar to those observed by MasCam are common on Ryugu.

Based on the low reflectivity, the flat spectral slope in the visible wavelengths and the inclusions identified in the rock imaged by MasCam, the rock appears to be similar to carbonaceous chondrites (Jaumann et al. 2019; Schröder et al. 2021; Otto et al. 2021). However, the analyses did not allow to constrain a specific type of carbonaceous chondrite confidently. Suggestions range from CI similar to the Tagish Lake meteorite (Jaumann et al. 2019) to CR or CV based on the relatively large size of the inclusions (Schröder et al. 2021) and also include the possibility that there is no Ryugu equivalent in our terrestrial meteorite collection (Grott et al. 2019; Schröder et al. 2021; Otto et al. 2021). ONC global data hints at thermally metamorphosed carbonaceous chondrites as an appropriate meteorite analogue given the dark nature of Ryugu's regolith (Sugita et al. 2019). Preliminary investigations of the returned samples suggest that based on their physical properties and bulk chemical composition, CI type carbonaceous chondrites appear to be having most similarities to Ryugu's samples (Tanaka et al. 2022; Yokoyama et al. 2022), but Ryugu has higher porosity, lower albedo and is more fragile in nature (Yada et al. 2022) and also is compositionally also nearly free of sulfates, ferrihydrites and interlayer water (Yokoyama et al. 2022). This evaluation is shared by the investigation of MARA of the Ryugu rock which is discussed in the following section.

Comparison with MARA

The thermal inertia of the rock at the MASCOT landing site of $256 (\pm 43) \text{ J m}^{-2} \text{ K}^{-1} \text{ s}^{-1/2}$ derived from MARA measurements (Hamm et al. 2018, 2022; Grott et al. 2019) is significantly lower than the value determined for the samples, which is $890 \pm 45 \text{ J m}^{-2} \text{ K}^{-1} \text{ s}^{-1/2}$ (at 298 K) (Nakamura et al. 2022). However, this discrepancy may be caused by the different scales on which the measurements have been taken (Nakamura et al. 2022). Furthermore, it is conceivable that the sampling process introduced a bias towards more consolidated material, while friable particles may have been shed off or destroyed in the process. In situ measurements by MASCOT may have probed material which could have been mechanically weakened by thermal fatigue. The induced cracks would result in a thermal inertia that was lower than that of the more consolidated returned samples.

Preliminary analysis of samples returned to Earth show that the average bulk density of Ryugu sample particles is $(1282 \pm 231) \text{ kg m}^{-3}$ (Yada et al. 2022), but later analysis taking the 3D shape of the particles into account arrive at higher densities between 1700 and 1900 kg m^{-3} (Nakamura et al. 2022). Assuming sample grain densities representative for CI and CM carbonaceous chondrites, the microporosity of Ryugu samples can be estimated to be close to 0.10 to 0.23 (Nakamura et al. 2022). This is much smaller than the value derived from in situ measurements (Grott et al. 2019) and the value favoured by Grott et al. (2020), which indicated high microporosities. This may be due to a selection bias for the samples, which need to exhibit some internal strength to survive the energetic sampling process.

To put MARA measurements into context, a summary of meteorite thermal conductivity as a function of porosity is shown in Fig. 6 together with estimates of thermal conductivity for the MASCOT rock and returned samples. The thermal conductivity k of the rock is derived from the measured thermal inertia Γ using

$$k = \frac{\Gamma^2}{\rho c_p} \quad (1)$$

where ρ is the bulk density and the heat capacity of the material calculated using Ryugu's average night time temperature of 230 K. The thermal conductivity has then been estimated assuming a heat capacity of $635 \text{ J kg}^{-1} \text{ K}^{-1}$ (Hemingway et al. 1973). The density ρ is determined from $\rho = (1 - \phi)\rho_s$, where ϕ is porosity and ρ_s the grain density, for which we assume values between 2120 and 2210 kg m^{-3} , representative for CI and CM chondrites, respectively (Nakamura et al. 2022). Using the models by Flynn et al., (2018) and Krause et al. (2011), we then derive porosities between 0.43 and,

resulting in thermal conductivities between $0.049 \text{ W m}^{-1} \text{ K}^{-1}$ and $0.146 \text{ W m}^{-1} \text{ K}^{-1}$. Spectral analysis of the returned samples shows an extremely dark optical to near-infrared reflectance and a spectral profile with weak absorptions at 2.7 and 3.4 μm (Pilorget et al. 2022; Yada et al. 2022). This implies the presence of hydrous minerals and organic matter and/or carbonate consistent with the spectral trend found by Hamm et al. (2022). Taken together and considering the absence of submillimetre CAIs and chondrules and the samples' bulk chemical composition (Yokoyama et al. 2022), these findings indicate that Ryugu is most similar to CI chondrites but has lower albedo and higher porosity. Considering that the thermal inertia and tensile strength of a material are both influenced by grain contacts, the thermal conductivity can be used to estimate the tensile strength σ_t (Grott et al. 2019) following the formula:

$$\sigma_t = \frac{\pi}{4000} \frac{k}{k_s} E \quad (2)$$

where k and k_s are the thermal conductivity of the bulk material and grain, respectively, and E is the Young's modulus. This results in an approximate tensile strength of 200–280 kPa for Ryugu's rock investigated by MARA (Grott et al. 2019) and ~ 229 kPa following the same approach applied to TIR data (Grott et al. 2019; Okada et al. 2020; Shimaki et al. 2020). To derive the tensile strength of the returned samples, Kurosawa et al. (2022) (also see (Nakamura et al. 2022)) conducted a three-point flexural bending test. They placed two $3 \times 3 \text{ mm}^2$ cut pieces of 0.788 mm and 0.950 mm thickness onto two bars of a testing machine and broke the samples by slowly pushing a piston down onto the sample while monitoring the load. They found a peak tensile strength between 3 and 8 MPa much higher than that of estimates using the thermal conductivity and MARA and TIR data. This discrepancy can be explained by the different size scales on which the tensile strength was derived. The tensile strength of brittle materials scales with $1/\sqrt{L}$ (Bažant 1999), where L is the characteristic length of the investigated sample. The size of the sample on which the tensile strength test has been conducted is about two orders of magnitude smaller than the characteristic length (a few thermal skin depths, \sim decimetre) of the rocks on Ryugu. Thus, considering the above-mentioned scaling relation, these values agree with each other (Biele et al. 2022).

Comparison with MasMag

Magnetic mineral characterization based on microscopic measurements of Ryugu samples show magnetite particles of various shapes (framboid, spherulite particles or dodecahedrons) and sizes (0.2–10 μm) (Dobrić et al.

2022; Yamaguchi et al. 2022) comprising 4–7% of the total grain volume (Yamaguchi et al. 2022). The measured mass specific susceptibility ($8.39 \times 10^{-5} \text{ m}^3/\text{kg}$), the saturation remanence/saturation magnetization ratio (0.09), and the coercivity of remanence/coercivity ratio (5) (Sato et al. 2022; Tanaka et al. 2022; Nakamura et al. 2022) corresponds to values similar to those observed in carbonaceous chondrites (e.g., Thorpe et al. 2002; Rochette et al. 2003; Sridhar et al. 2021). The particles were also characterized magnetically in terms of low-temperature remanence cycles, isothermal remanence gradient curve, and first-order reversal curve measurements, indicating that the fine-grained framboidal magnetite, coarse-grained magnetite, and pyrrhotite are dominant ferromagnetic minerals in Ryugu particles (Sato et al. 2022). The natural remanence measurements of two Ryugu particles of 0.1–1 mm scale show stable vector components with a total specific moment of $\sim 10^{-2} \text{ Am}^2/\text{kg}$, and the stable components are likely carried by the framboidal magnetite (Sato et al. 2022; Nakamura et al. 2022). The value corresponds well to the specific magnetic moment of chondrites. The lithological structure of the returned samples indicates that the magnetization scale is likely within the scale of the brecciated domain size of a few 100s of micrometres as these are randomly distributed in the matrix. This is consistent with the observations that the remanence intensity of 0.1–1 mm sized materials ($\sim 10^{-2} \text{ Am}^2/\text{kg}$ (Sato et al. 2022)) is orders of magnitude larger than those of decimetre sized materials ($\sim 10^{-5} \text{ Am}^2/\text{kg}$ (Hercik et al. 2020)).

Discussion

A primary scientific objective of MASCOT was to provide a link between orbiter observations of the asteroid Ryugu and the samples returned from it by conducting in situ asteroid science. Table 1 lists the measurements conducted by MASCOT and their corresponding findings from the returned samples and the orbiter instruments where available. Most of the listed properties could be derived from MasCam and MARA. Properties that agree at all scales, from the returned sample, in situ and orbiter investigations include characteristics derived from images, such as the surface texture of particles/boulders, the colour in the visible wavelength, and the potential meteorite analogue (suggested to be a CI carbonaceous chondrite), as well as characteristics derived from thermal measurements, such as density, porosity and closest meteorite analogue.

In general, MASCOT's observations appear to have a greater overlap with orbiter observations, including the reflectance in the visible wavelengths, thermal inertia and derived tensile strength, compared to returned

samples measured at smaller scales. This seems to imply that at a spatial scale below MASCOT's resolution (sub-millimetre to centimetre), these properties increase in magnitude. With returned particles being several millimetres in size at most, the scale at which the reflectance and thermal inertia (and the derived scale-dependent tensile strength) change appears to be in the millimetre range. Indeed, this range also describes the scale, and below, at which roughness begins to dominate the photometric behaviour of a regolith (Labarre et al. 2017). The scale also represents the diurnal skin depth of Ryugu regolith ($\sim 3\text{--}10 \text{ mm}$ (Hamm et al. 2022)), the characteristic length scale for thermal measurements. Thus, it is not surprising that measurements from MASCOT and the returned samples differ and the spatial scale at which this difference occurs is in agreement with MASCOT's observations.

There is a divergence of the particle size frequency distributions observed on different scales. While MasCam did not see any grains or fine particles, the power index of boulders $> 5 \text{ m}$ is much smaller than the one of the returned sample fragments, possibly caused by further fragmentation of the samples during and after the sampling process (Yada et al. 2022). This can also explain why there are no particles visible in the MasCam images equivalently sized to the returned sample fragments. Another possible explanation for the absence of fine particles at the MASCOT landing site is that fine grains may be present inside pores (Morota et al. 2020) and are thus not visible in images from MasCam.

MasCam identified inclusions (Jaumann et al. 2019), while the returned samples are depleted in inclusions (Yada et al. 2022), but no equivalent observation could be made by the orbiter because of its lower spatial resolution. Due to the presence of different rock types on Ryugu that have been identified by ONC and MasCam data (Sugita et al. 2019; Jaumann et al. 2019), it cannot be excluded that the rock imaged by MasCam is of a different type than the returned samples. In addition, some of the identified inclusions could also be specular reflections (Yumoto et al. 2022; Schröder et al. 2022).

In all cases in which the orbiter and returned sample observations agree, MASCOT confirmed these observations and thus links meter and sub-millimetre scale observations. However, there are also some observations that are unique to MASCOT, such as the detection of inclusions/clasts in the rock at MASCOT's landing site and absence of fine particles on the asteroid surface (Jaumann et al. 2019). Although it can be assumed that the returned samples are generally a good representative of Ryugu's regolith in terms of their morphology and composition (Yada et al. 2022; Tachibana et al. 2022), MASCOT shows that heterogeneities within the rock and on

the asteroid surface exist on millimetre scales. Although some of MASCOT's unique observations could also be retrieved from more returned sample material, this is not a highly ranked requirement for future missions given that Earth-based analytical methods can be performed on much smaller samples (Sawada et al. 2017). Thus, MASCOT has proven to be a valuable addition to the Hayabusa2 mission providing additional scientific output, confirming observations, and bridging the gap in spatial resolution between the orbiter and the returned samples. MASCOT provides critical in situ context for the returned samples and confirms the value of including surface science packages on future sample return missions (Ulamiec et al. 2014; Lange et al. 2018).

Conclusion

We have revisited the findings of the MASCOT lander onboard Hayabusa2 that was delivered to the surface of asteroid Ryugu and related its scientific findings to those of the returned samples and the orbiter instruments. MASCOT's in situ observations on centimetre to millimetre spatial scales has proven to be a valuable link between orbiter observations and laboratory investigations of the returned samples. MASCOT allowed a close view of undisturbed surface material of a C-type asteroid, a first measurement of its kind. While confirming some observations, such as the surface texture of particles/boulders, the colour in the visible wavelength, the density, the porosity and the type of potential meteorite analogue, MASCOT has also provided knowledge about inclusions in rocks and the presence of dust-free surfaces at scales that could not be retrieved from the returned samples and the Hayabusa2 orbiter. We conclude that the delivery of a lander on a planetary body provides valuable information that supports remote sensing as well as returned sample analyses.

Abbreviations

CAI	Calcium–aluminium-rich inclusions
LED	Light emitting diode
MARA	MASCOT Radiometer
MasCam	MASCOT Camera
MASCOT	Mobile Asteroid Surface Scout
MasMag	MASCOT Magnetometer
MicrOmega	MASCOT Hyperspectral Microscope
ONC	Optical Navigation Camera
TIR	Thermal Infrared Imager
NIRS3	Near Infrared Spectrometer
SCI	Small Carry-on Impactor
RMS	Root Mean Square

Acknowledgements

We gratefully acknowledge the dedication and commitment of the Hayabusa2 and MASCOT teams that made this work possible. We thank two anonymous reviewers for their helpful comments.

Author contributions

K.A.O. coordinated co-author contributions, led interpretations and compiled the article. M.G., D.H., M.H., T.-M.H., R.J., M.S. and S.U. contributed to the writing. J.B., J.K., T.N., S.E.S., S.T. and H.Y. contributed to the interpretation and provided information on specific topics. All authors discussed the results and commented on the manuscript. All authors read and approved the final manuscript.

Funding

Open Access funding enabled and organized by Projekt DEAL. The team acknowledges funding by DLR and CNES.

Availability of data and materials

This manuscript is based on previously published data. Please refer to the quoted references for details.

Declarations

Ethics approval and consent to participate

Not applicable.

Consent for publication

Not applicable.

Competing interests

The authors declare that they have no known competing financial interests or personal relationships that could have appeared to influence the work reported in this paper.

Author details

¹German Aerospace Center (DLR), Institute of Planetary Research, Berlin, Germany. ²Hiroshima University, Department of Earth and Planetary Systems Science, Higashi-Hiroshima, Japan. ³German Aerospace Center (DLR), Institute of Space Systems, Bremen, Germany. ⁴German Aerospace Center (DLR), Space Operations and Astronaut Training, Cologne, Germany. ⁵Institute d'Astrophysique Spatiale, Orsay, France. ⁶Free University Berlin, Institute of Geological Sciences, Berlin, Germany. ⁷Institute of Atmospheric Physics (CAS), Prague, Czech Republic. ⁸University of Tokyo, Department of Earth and Planetary Science, Tokyo, Japan. ⁹Luleå University of Technology, Department of Computer Science, Electrical and Space Engineering, Kiruna, Sweden. ¹⁰Japan Aerospace Exploration Agency (JAXA), Institute of Space and Astronautical Science (ISAS), Sagami-hara, Japan. ¹¹Technical University Braunschweig, Institute of Geophysics and Extraterrestrial Physics, Brunswick, Germany. ¹²University of Aizu, Center for Advanced Information Science and Technology (CAIST), Fukushima, Japan. ¹³Centre National d'Etudes Spatiales (CNES), Toulouse, France. ¹⁴Tohoku University, Department of Earth Sciences, Sendai, Japan. ¹⁵Planetary Exploration Research Center, Chiba Institute of Technology, Chiba, Japan.

Received: 26 August 2022 Accepted: 27 February 2023

Published online: 06 April 2023

References

- Acuña MH, Anderson BJ, Russell CT et al (2002) NEAR Magnetic Field Observations at 433 Eros: first Measurements from the Surface of an Asteroid. *Icarus* 155:220–228. <https://doi.org/10.1006/icar.2001.6772>
- Arakawa M, Saiki T, Wada K et al (2020) An artificial impact on the asteroid (162173) Ryugu formed a crater in the gravity-dominated regime. *Science* 368:67–71. <https://doi.org/10.1126/science.aaz1701>
- Astromaterials Science Research Group (ASRG) (2022) Institute of Space and Astronautical Science (ISAS), Japan Aerospace Exploration Agency (JAXA), CNES TIDS (IAS): Hayabusa2, Ryugu Sample Curatorial Dataset. <https://doi.org/10.17597/ISAS.DARTS/CUR-Ryugu-description>
- Auster H-U, Apathy I, Berghofer G et al (2015) The nonmagnetic nucleus of comet 67P/Churyumov-Gerasimenko. *Science* 349:5102. <https://doi.org/10.1126/science.aaa5102>

- Bažant ZP (1999) Size effect on structural strength: a review. *Arch Appl Mech* 69:703–725. <https://doi.org/10.1007/s004190050252>
- Bibring J-P, Hamm V, Langevin Y et al (2017) The MicrOmega Investigation Onboard Hayabusa2. *Space Sci Rev* 208:401–412. <https://doi.org/10.1007/s11214-017-0335-y>
- Bibring J-P, Pilorget C, Riu L et al (2022) MicrOmega/MASCOT first results. *Planet Space Sci* 210:105393. <https://doi.org/10.1016/j.pss.2021.105393>
- Biele J, Kührt E, Senshu H et al (2019) Effects of dust layers on thermal emission from airless bodies. *Prog Earth Planet Sci* 6:48. <https://doi.org/10.1186/s40645-019-0291-0>
- Biele J, Vincent J-B, Knollenberg J (2022) Mechanical properties of cometary surfaces. *Universe* 8:487. <https://doi.org/10.3390/universe8090487>
- Dobrică E, Ishii HA, Bradley JP, et al (2022) Nanoscale Investigation of Various Magnetite Morphologies in the Samples Returned from C-Type Asteroid Ryugu: Insights into the Aqueous Alteration Processes. In: 53rd Lunar and Planetary Science Conference. LPI Contribution No. 2678, The Woodlands, Texas, USA, 7–11 March 2022, #2188
- Flynn GJ, Consolmagno GJ, Brown P, Macke RJ (2018) Physical properties of the stone meteorites: Implications for the properties of their parent bodies. *Geochemistry* 78:269–298. <https://doi.org/10.1016/j.chemer.2017.04.002>
- Gattacceca J, Rochette P (2004) Toward a robust normalized magnetic paleointensity method applied to meteorites. *Earth Planet Sci Lett* 227:377–393. <https://doi.org/10.1016/j.epsl.2004.09.013>
- Grott M, Knollenberg J, Borgs B et al (2017) The MASCOT radiometer MARA for the Hayabusa 2 mission. *Space Sci Rev* 208:413–431. <https://doi.org/10.1007/s11214-016-0272-1>
- Grott M, Knollenberg J, Hamm M et al (2019) Low thermal conductivity boulder with high porosity identified on C-type asteroid (162173) Ryugu. *Nat Astron* 3:971–976. <https://doi.org/10.1038/s41550-019-0832-x>
- Grott M, Biele J, Michel P et al (2020) Macroporosity and grain density of rubble pile asteroid (162173) Ryugu. *J Geophys Res: Planets* 125:6519. <https://doi.org/10.1029/2020JE006519>
- Hamm M, Grott M, Kührt E et al (2018) A method to derive surface thermophysical properties of asteroid (162173) Ryugu (1999JU3) from in-situ surface brightness temperature measurements. *Planet Space Sci* 159:1–10. <https://doi.org/10.1016/j.pss.2018.03.017>
- Hamm M, Pelivan I, Grott M, de Wiljes J (2020) Thermophysical modelling and parameter estimation of small Solar system bodies via data assimilation. *Mon Not R Astron Soc* 496:2776–2785. <https://doi.org/10.1093/mnras/staa1755>
- Hamm M, Grott M, Senshu H et al (2022) Mid-infrared emissivity of partially dehydrated asteroid (162173) Ryugu shows strong signs of aqueous alteration. *Nat Commun* 13:364. <https://doi.org/10.1038/s41467-022-28051-y>
- Hemingway BS, Robie RA, Wilson WH (1973) Specific heats of lunar soils, basalt, and breccias from the Apollo 14, 15, and 16 landing sites, between 90 and 350°K. *Lunar and Planetary Science Conference Proceedings*. 4:2481
- Herbst W, Greenwood JP, Yap TE (2021) The Macroporosity of Rubble Pile Asteroid Ryugu and Implications for the Origin of Chondrules. *Planet Sci J* 2:110. <https://doi.org/10.3847/PSJ/abf7c0>
- Herbst W, Greenwood JP (2022) Why are chondrules rare or absent in the Ryugu samples? In: 53rd Lunar and Planetary Science Conference. LPI Contribution No. 2678, The Woodlands, Texas, USA, 7–11 March 2022, #1589
- Herčík D, Auster H-U, Blum J et al (2017) The MASCOT Magnetometer. *Space Sci Rev* 208:433–449. <https://doi.org/10.1007/s11214-016-0236-5>
- Hercik D, Auster H-U, Constantinescu D et al (2020) Magnetic properties of asteroid (162173) Ryugu. *J Geophys Res: Planets* 125:6035. <https://doi.org/10.1029/2019JE006035>
- Ho T-M, Baturkin V, Grimm C et al (2017) MASCOT—the mobile asteroid surface scout onboard the Hayabusa2 mission. *Space Sci Rev* 208:339–374. <https://doi.org/10.1007/s11214-016-0251-6>
- Ho T-M, Jaumann R, Bibring J-P et al (2021) The MASCOT lander aboard Hayabusa2: the in-situ exploration of NEA (162173) Ryugu. *Planet Space Sci*. <https://doi.org/10.1016/j.pss.2021.105200>
- Ito M, Tomioka N, Uesugi M et al (2022) A pristine record of outer Solar System materials from asteroid Ryugu's returned sample. *Nat Astron* 6:1163–1171. <https://doi.org/10.1038/s41550-022-01745-5>
- Iwata T, Kitazato K, Abe M et al (2017) NIRS3: the near infrared spectrometer on Hayabusa2. *Space Sci Rev* 208:317–337. <https://doi.org/10.1007/s11214-017-0341-0>
- Jaumann R, Schmitz N, Koncz A et al (2017) The camera of the MASCOT asteroid lander on board Hayabusa 2. *Space Sci Rev* 208:375–400. <https://doi.org/10.1007/s11214-016-0263-2>
- Jaumann R, Schmitz N, Ho T-M et al (2019) Images from the surface of asteroid Ryugu show rocks similar to carbonaceous chondrite meteorites. *Science* 365:817–820. <https://doi.org/10.1126/science.aaw8627>
- Kameda S, Suzuki H, Takamatsu T et al (2017) Preflight calibration test results for optical navigation camera telescope (ONC-T) onboard the Hayabusa2 spacecraft. *Space Sci Rev* 208:17–31. <https://doi.org/10.1007/s11214-015-0227-y>
- Kitazato K, Milliken RE, Iwata T et al (2019) The surface composition of asteroid 162173 Ryugu from Hayabusa2 near-infrared spectroscopy. *Science* 364:272–275. <https://doi.org/10.1126/science.aav7432>
- Krause M, Blum J, Skorov YuV, Trierloff M (2011) Thermal conductivity measurements of porous dust aggregates: I. technique, model and first results. *Icarus* 214:286–296. <https://doi.org/10.1016/j.icarus.2011.04.024>
- Kurosawa K, Tanaka S, Ino Y, et al (2022) Tensile (Flexural) Strength of Ryugu Grain C0002. In: 53rd Lunar and Planetary Science Conference. LPI Contribution No. 2678, The Woodlands, Texas, USA, 7–11 March 2022, #1378
- Labarre S, Ferrari C, Jacquemoud S (2017) Surface roughness retrieval by inversion of the Hapke model: a multiscale approach. *Icarus* 290:63–80. <https://doi.org/10.1016/j.icarus.2017.02.030>
- Lange C, Ho T-M, Grimm CD et al (2018) Exploring small bodies: nano- and microlander options derived from the mobile asteroid surface scout. *Adv Space Res* 62:2055–2083. <https://doi.org/10.1016/j.asr.2018.05.013>
- Lange C, Yoshimitsu T, Ulamec S et al (2020) Micro- and nanolander on the surface of Ryugu – Commonalities, differences and lessons learned for future microgravity exploration. *Planet Space Sci* 194:105094. <https://doi.org/10.1016/j.pss.2020.105094>
- Michikami T, Honda C, Miyamoto H et al (2019) Boulder size and shape distributions on asteroid Ryugu. *Icarus* 331:179–191. <https://doi.org/10.1016/j.icarus.2019.05.019>
- Morota T, Sugita S, Cho Y et al (2020) Sample collection from asteroid (162173) Ryugu by Hayabusa 2: Implications for surface evolution. *Science* 368:654–659. <https://doi.org/10.1126/science.aaz6306>
- Nakamura T, Matsumoto M, Amano K et al (2022) Formation and evolution of carbonaceous asteroid Ryugu: direct evidence from returned samples. *Science*. <https://doi.org/10.1126/science.abn8671>
- Okada T, Fukuhara T, Tanaka S et al (2017) Thermal infrared imaging experiments of C-type asteroid 162173 Ryugu on Hayabusa2. *Space Sci Rev* 208:255–286. <https://doi.org/10.1007/s11214-016-0286-8>
- Okada T, Fukuhara T, Tanaka S et al (2020) Highly porous nature of a primitive asteroid revealed by thermal imaging. *Nature*. <https://doi.org/10.1038/s41586-020-2102-6>
- Otto KA, Matz K-D, Schröder SE et al (2020) Surface roughness of asteroid (162173) Ryugu and comet 67P/Churyumov–Gerasimenko inferred from in situ observations. *Mon Not R Astron Soc* 500:3178–3193. <https://doi.org/10.1093/mnras/staa3314>
- Otto KA, Schröder SE, Scharf HD et al (2021) Spectral and petrographic properties of inclusions in carbonaceous chondrites and comparison with in situ images from asteroid Ryugu. *Planet Sci J* 2:188. <https://doi.org/10.3847/PSJ/ac034b>
- Pilorget C, Okada T, Hamm V et al (2022) First compositional analysis of Ryugu samples by the MicrOmega hyperspectral microscope. *Nat Astron* 6:221–225. <https://doi.org/10.1038/s41550-021-01549-z>
- Rochette P, Sagnotti L, Bourot-Denise M et al (2003) Magnetic classification of stony meteorites: 1 Ordinary Chondrites. *Meteorit Planet Sci* 38:251–268. <https://doi.org/10.1111/j.1945-5100.2003.tb00263.x>
- Sakatani N, Tanaka S, Okada T et al (2021) Anomalously porous boulders on (162173) Ryugu as primordial materials from its parent body. *Nat Astron* 5:766–774. <https://doi.org/10.1038/s41550-021-01371-7>
- Sato M, Kimura Y, Tanaka S et al (2022) Rock Magnetic Characterization of Returned Samples From Asteroid (162173) Ryugu: Implications for Paleomagnetic Interpretation and Paleointensity Estimation. *J Geophys Res: Planets* 127:e2022JE7405. <https://doi.org/10.1029/2022JE007405>
- Sawada H, Okazaki R, Tachibana S et al (2017) Hayabusa2 Sampler: collection of asteroidal surface material. *Space Sci Rev* 208:81–106. <https://doi.org/10.1007/s11214-017-0338-8>
- Scholten F, Preusker F, Elgner S et al (2019) The Hayabusa2 lander MASCOT on the surface of Asteroid (162173) Ryugu - Stereo-photogrammetric

- analysis of MASCam image data. *A&A* 632:1–6. <https://doi.org/10.1051/0004-6361/201936760>
- Schröder S, Otto K, Scharf H et al (2021) Spectrophotometric analysis of the Ryugu rock seen by MASCOT: searching for a carbonaceous chondrite analog. *Planet Sci J* 2:58. <https://doi.org/10.3847/PSJ/abbb97>
- Schröder S, Sakatani N, Honda R et al (2022) Characterization of the MASCOT landing area by Hayabusa2. *A&A* 666:A164. <https://doi.org/10.1051/0004-6361/202244059>
- Shimaki Y, Senshu H, Sakatani N et al (2020) Thermophysical properties of the surface of asteroid 162173 Ryugu: infrared observations and thermal inertia mapping. *Icarus* 348:113835. <https://doi.org/10.1016/j.icarus.2020.113835>
- Sridhar S, Bryson JFJ, King AJ, Harrison RJ (2021) Constraints on the ice composition of carbonaceous chondrites from their magnetic mineralogy. *Earth Planet Sci Lett* 576:117243. <https://doi.org/10.1016/j.epsl.2021.117243>
- Sugita S, Honda R, Morota T et al (2019) The geomorphology, color, and thermal properties of Ryugu: Implications for parent-body processes. *Science* 364:1–11. <https://doi.org/10.1126/science.aaw0422>
- Tachibana S (2019) Hayabusa2: sample acquisition at a near-earth C-type Asteroid Ryugu and analysis plan of returned samples. *Microsc Microanal* 25:2442–2443. <https://doi.org/10.1017/S1431927619012947>
- Tachibana S, Sawada H, Okazaki R et al (2022) Pebbles and sand on asteroid (162173) Ryugu: in situ observation and particles returned to Earth. *Science* 375:1011–1016. <https://doi.org/10.1126/science.abj8624>
- Tanaka S, Nagano H, Yagi T, et al (2022) Physical properties of the returned sample of Ryugu by Hayabusa2 mission. In: 53rd Lunar and Planetary Science Conference. LPI Contribution No. 2678, The Woodlands, Texas, USA, 7–11 March 2022, #1373
- Tatsumi E, Domingue D, Yokota Y et al (2020) Global photometric properties of (162173) Ryugu. *Astron Astrophys* 639:1–19. <https://doi.org/10.1051/0004-6361/201937096>
- Tatsumi E, Sakatani N, Riu L et al (2021) Spectrally blue hydrated parent body of asteroid (162173) Ryugu. *Nat Commun* 12:5837. <https://doi.org/10.1038/s41467-021-26071-8>
- Terho M, Pesonen LJ, Kukkonen IT (1996) Magnetic properties of asteroids from meteorite data — Implications for magnetic anomaly detections. *Earth Moon Planet* 72:225–231. <https://doi.org/10.1007/BF00117522>
- Thorpe AN, Senftle FE, Grant JR (2002) Magnetic study of magnetite in the Tagish Lake meteorite. *Meteorit Planet Sci* 37:763–771. <https://doi.org/10.1111/j.1945-5100.2002.tb00853.x>
- Tsuchiyama A, Matsumoto M, Matsuno J, et al (2022) Mineralogical, Petrological, and Physical Properties of Ryugu Samples Using X-Ray Nanotomography. In: 53rd Lunar and Planetary Science Conference. LPI Contribution No. 2678, The Woodlands, Texas, USA, 7–11 March 2022, #1858
- Ulamiec S, Biele J, Bousquet P-W et al (2014) Landing on small bodies: from the Rosetta Lander to MASCOT and beyond. *Acta Astronaut* 93:460–466. <https://doi.org/10.1016/j.actaastro.2013.02.007>
- Watanabe S, Tsuda Y, Yoshikawa M et al (2017) Hayabusa2 mission overview. *Space Sci Rev* 208:3–16. <https://doi.org/10.1007/s11214-017-0377-1>
- Watanabe S, Hirabayashi M, Hirata N et al (2019) Hayabusa2 arrives at the carbonaceous asteroid 162173 Ryugu - A spinning top-shaped rubble pile. *Science* 364:268–272. <https://doi.org/10.1126/science.aav8032>
- Yada T, Abe M, Okada T et al (2022) Preliminary analysis of the Hayabusa2 samples returned from C-type asteroid Ryugu. *Nat Astron* 6:214–220. <https://doi.org/10.1038/s41550-021-01550-6>
- Yamaguchi A, Kimura M, Ito M, et al (2022) Petrology of Asteroid Ryugu particles Allocated to the Phase2 Curation Kochi Team. In: 53rd Lunar and Planetary Science Conference. LPI Contribution No. 2678, The Woodlands, Texas, USA, 7–11 March 2022, #1822
- Yokoyama T, Nagashima K, Nakai I, et al (2022) Samples returned from the asteroid Ryugu are similar to Ivuna-type carbonaceous meteorites. *Science* 0:eabn7850. <https://doi.org/10.1126/science.abn7850>
- Yumoto K, Cho Y, Yabe Y, et al (2022) Visible Multi-Band Spectra and Specular Reflectivity of Ryugu Returned Samples. In: 53rd Lunar and Planetary Science Conference. LPI Contribution No. 2678, The Woodlands, Texas, USA, 7–11 March 2022, #1326

Publisher's Note

Springer Nature remains neutral with regard to jurisdictional claims in published maps and institutional affiliations.

Submit your manuscript to a SpringerOpen® journal and benefit from:

- Convenient online submission
- Rigorous peer review
- Open access: articles freely available online
- High visibility within the field
- Retaining the copyright to your article

Submit your next manuscript at ► [springeropen.com](https://www.springeropen.com)